Seasonal ice dynamics control the timing of crevasse drainage at a fast-flowing outlet glacier

Thomas R. Chudley
Department of Geographical Sciences, University of Bristol, Bristol, UK
https://orcid.org/0000-0001-8547-1132

Chris R. Stokes
Department of Geography, Durham University, Durham, UK
https://orcid.org/0000-0003-3355-1573

James M. Lea
Department of Geography and Planning, University of Liverpool, Liverpool UK
https://orcid.org/0000-0003-1885-0858

Thomas Winterbottom
Department of Computer Science, Durham University, Durham, UK
https://orcid.org/0000-0001-9976-3689

Robert Law
Laboratory of Hydraulics, Hydrology and Glaciology (VAW), ETH Zurich, Zurich, Switzerland
Swiss Federal Institute for Forest, Snow and Landscape Research (WSL), Sion, Switzerland
https://orcid.org/0000-0003-0067-5537

Caroline C. Clason
Department of Geography, Durham University, Durham, UK
https://orcid.org/0000-0001-8236-2555

Holly E. Wytiahlowsky
Department of Geography, Durham University, Durham, UK
https://orcid.org/0000-0002-5631-3677

Jack L. Dechow
Department of Earth, Marine and Environmental Sciences, University of North Carolina, USA
https://orcid.org/0000-0003-3121-7934

Corresponding author: Thomas R. Chudley (tom.chudley@bristol.ac.uk)

This is a preprint submitted to EarthArXiv and has not been peer reviewed

Seasonal ice dynamics control the timing of crevasse drainage at a fast-flowing outlet glacier

T. R. Chudley[1,2], C. R. Stokes[2], J. M. Lea[3], T. Winterbottom[4], R. Law[5,6], C. C. Clason[2], H. E. Wytiahlowsky[2], J. L. Dechow[7]

[1] Department of Geographical Sciences, University of Bristol, Bristol, UK
[2] Department of Geography, Durham University, Durham, UK
[3] Department of Geography and Planning, University of Liverpool, Liverpool UK
[4] Department of Computer Science, Durham University, Durham, UK
[5] Laboratory of Hydraulics, Hydrology and Glaciology (VAW), ETH Zurich, Zurich, Switzerland
[6] Swiss Federal Institute for Forest, Snow and Landscape Research (WSL), Sion, Switzerland
[7] Department of Earth, Marine and Environmental Sciences, University of North Carolina, USA

Corresponding author: Thomas Chudley (thomas.r.chudley@durham.ac.uk)

KEY POINTS

- Satellite observations indicate ponded crevasse fields drain with seasonal peaks in strain rates suggesting a dynamic control.
- Where meltwater is not limited, hydrofracture modelling supports that seasonal acceleration can trigger crevasse drainage.
- This behaviour is distinct from the short-term and transient mechanisms thought to trigger supraglacial lake drainage.

ABSTRACT

Crevasse field drainage transfers at least half of the seasonal runoff from the surface to the bed of the Greenland Ice Sheet, but the patterns of drainage are complex and spatio-temporally heterogenous. To better understand controls on crevasse drainage processes, we use an automated deep learning method to map the seasonal filling and drainage of water-filled crevasses at Sermeq Kujalleq (Store Glacier) in 2019 using 10-metre-resolution Sentinel-2 MSI imagery, alongside RACMO reanalysis melt estimates and strain rates inferred from ITS_LIVE velocity observations. The timing of crevasse drainage correlates strongly with seasonal peaks in surface strain rates, suggesting that seasonal variation in surface stress exerts a strong control on the exact timing of drainage to the bed. Linear elastic fracture mechanics (LEFM) modelling suggests that a seasonal transition to higher tensile stress regimes can trigger rapid full-depth hydrofracture at the point at which stresses exceed the threshold necessary to initiate initial fracture, provided that meltwater from early-season snowmelt is abundant. We suggest that this causal behaviour is distinct from both (i) supraglacial lake drainage, which depends on short-term (hourly-daily) transient accelerations to trigger drainage; and (ii) crevasse fields that are not observed to pond, which exist in high tensile regimes and likely readily supply water into the englacial or subglacial system from melt-season onset. The distinct mode of drainage described here requires unique

parameterisation to predict spatio-temporal patterns of water transfer to the bed of ice sheets and drive models of subglacial hydrology.

PLAIN LANGUAGE SUMMARY

Meltwater produced on the surface of the Greenland Ice Sheet flows into and beneath the ice sheet before reaching the ocean. At least half of this meltwater is transferred through crevasse fields, regions of open fracture in the ice surface, but satellite observations show the distribution of meltwater in crevasse fields to be highly variable in space and time. We track water filling and drainage in crevasse fields from satellite imagery, and show that crevasse drainages appear to occur alongside seasonal peaks in the ice surface strain rate. We suggest that, as the melt season progresses and the glacier speeds up, increasing tensile stresses eventually trigger the drainage of ponded crevasses. This is distinct from the drainage of ice-surface lakes, which do not exhibit a seasonal increase in strain rates and instead depend on short-term accelerations (due to e.g. rainfall events) to trigger drainage. This may also explain why large regions of crevasse fields are not observed to pond: extensional stresses here are high throughout the season, allowing water to drain before it fills to the surface. Incorporating the disparate effects of these seasonal stress variations into models of meltwater transport will help us better represent complex ice sheet hydrology.

1. INTRODUCTION

Of the hundreds of Gigatonnes of surface runoff produced across the Greenland Ice Sheet (GrIS) each year (T. Slater et al., 2021), the majority is transported to the ocean through the englacial and subglacial environment (Gantayat et al., 2023; Koziol et al., 2017). As meltwater is routed through the ice sheet, a number of second-order processes can act to alter ice sheet dynamics. The conversion of latent heat into thermal energy can act to soften ice rheology (Bell et al., 2014; Colgan et al., 2015; Phillips et al., 2010), and the conversion of gravitational potential energy can increase basal melt rates (Young et al., 2022). Diurnal and seasonal velocities can also be significantly influenced by the impact of subglacial hydrology on effective pressure and ice flow, even at fast-flowing marine-terminating outlets (Cook et al., 2022; Moon et al., 2014; Sommers et al., 2024; Stevens et al., 2022; Vijay et al., 2019). Furthermore, at marine-terminating margins, meltwater plumes releasing meltwater into the fjord can act to promote calving and frontal melt (Cowton et al., 2015; D. A. Slater & Straneo, 2022). A better understanding of the spatio-temporal distribution of meltwater routing across, through and beneath ice sheets is therefore key to be able to predict these feedbacks (Banwell et al., 2016).

A notable hydrological feature in Greenland, particularly at fast-flowing outlet glaciers, are the presence of annually recurring, seasonally draining, ponded crevasse fields (Chudley et al., 2021; Everett et al., 2016; Lampkin et al., 2013, 2018), distinct in context and morphology from the more intensively studied supraglacial lake drainage events (Doyle et al., 2013; Stevens et al., 2015). Although most common in the ablation zone, where 25% of crevasse fields have been observed to exhibit ponding (Chudley et al., 2021), observations and modelling suggest that crevasse drainage

to the ice sheet bed can even extend to firn aquifers inland (Mejia et al., 2025; Poinar et al., 2017). These phenomena are likely important for controlling the spatio-temporal distribution of meltwater delivery to the bed: surface routing models suggest that crevasse fields capture anywhere from half (Koziol et al., 2017) to nearly all (Gantayat et al., 2023) of total runoff, with crevasses capturing higher proportions of meltwater at marine-terminating outlets. The extent and depth of crevasses have been observed to be increasing at accelerating ice sheet margins (Chudley et al., 2025; Colgan et al., 2011), suggesting that crevasse drainage may become an even larger component of the surface-to-bed drainage system in the future.

Modelling studies have suggested that the drainage of ponded crevasse fields is likely sufficient to significantly alter basal water pressures, with implications for glacier sliding (Cavanagh et al., 2017; McGrath et al., 2011; Poinar et al., 2019). However, being able to properly parameterise the process into regional-scale models of ice sheet hydrology and dynamics is challenging because the exact controls on the distribution and timing of drainage are poorly understood. Where hydrological routing models parameterise crevasse drainage, spatially uniform behaviour is assumed across crevassed regions, whether as fill-drain cycles analogous to lakes (Clason et al., 2015; Gantayat et al., 2023) or as distributed meltwater fed directly to the bed (Koziol et al., 2017; Sommers et al., 2024). However, limited observational evidence suggests that the filling and drainage of ponded crevasse fields is in fact spatio-temporally heterogenous, collected in discrete clusters (Lampkin et al., 2013) and likely controlled by ice dynamics rather than meltwater availability (Chudley et al., 2021; Everett et al., 2016). Parameterising these processes into models requires a more complete understanding of the temporal and spatial controls on ponded crevasse drainage.

Here, we use remotely sensed observations, supported by modelling, to explore the impact of seasonally varying ice dynamics on the distribution and drainage of ponded crevasse fields. Whilst observational studies of supraglacial lakes have suggested that short-term (< 24 hr) transient variations in ice dynamics, rather than seasonal trends, trigger drainage (Christoffersen et al., 2018; Poinar & Andrews, 2021; Stevens et al., 2015), the strong relationship between compressive background stress and observed crevasse ponding (Chudley et al., 2021) suggest that ice dynamics may have a different mechanical relationship with hydrofracture in ponded crevasse fields. We hypothesise that: (1) the seasonal evolution of ice dynamics exerts a control on the timing of crevasse drainage, (2) which is mechanically distinct to that associated with supraglacial lakes, requiring distinct parameterisation in regional models of ice sheet hydrology.

2. METHODS

2.1 Study Area

We focus on a 52 × 40 km study area (EPSG:3413 bounds: -214,000 m, -2,142,000 m, -162,000 m, -2,102,000 m) on Sermeq Kujalleq (Store Glacier), a marine-terminating outlet glacier in West Greenland (Figure 1; hereafter SKSG). SKSG was selected because it has an active surface

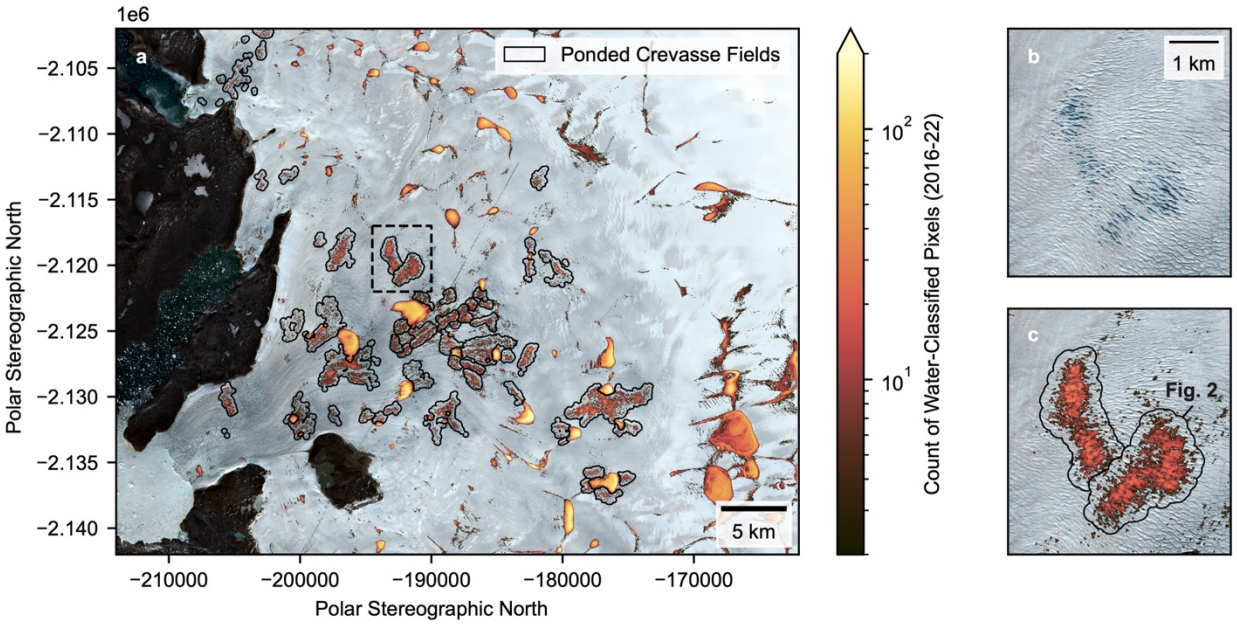

Figure 1. *(a) Overview of Sermeq Kujalleq (Store Glacier) study region, showing the number of times individual pixels were classified as water through the study period (counts > 1 are shown). Black lines mark the automatically-detected boundaries of contiguous ponded crevasse fields (see Methods). Dashed black indicates location of panels b-c. (b) Example of ponded crevasse field. (c) Example of classified ponded crevasse fields bounds, with water-classified pixel counts matching panel a. Crevasse field used for Figure 2 is labelled. Background image: Sentinel-2 scene dated 2019-06-01.*

hydrological system including seasonally draining supraglacial lakes (Chudley et al., 2019; Williamson, Willis, et al., 2018) and crevasse fields (Chudley et al., 2021; Kendrick et al., 2018). Surface meltwater inputs across SKSG have also been shown to play an important role in modulating subglacial water pressures, which act to control seasonal ice dynamics (Cook et al., 2020; Doyle et al., 2018; Howat et al., 2010). Meltwater at SKSG has also been shown to drive substantial basal melt rates (Young et al., 2022) and deliver meltwater to the glacier front, where plumes can drive frontal melt and calving activity (Cook et al., 2020, 2022).

2.2 Water Classification

We classify surface water in 10 m Sentinel-2 multispectral imagery using a U-net (Fig. S1), a convolutional neural network (CNN) architecture that performs well in semantic segmentation tasks for computer vision (Ronneberger et al., 2015). U-nets are now well-established for glaciological remote sensing problems, including the detection of supraglacial lakes (Lutz et al., 2023) and ice shelf damage (Surawy-Stepney et al., 2023). Water detection methods based around pixel thresholding, such as the Normalised Difference Water Index (NDWI), are well-established approaches for observing the GrIS from medium-resolution optical satellite imagery (Williamson, Banwell, et al., 2018). However, these methods are less sensitive to high-spatial-frequency features such as crevasses and streams that frequently occur with widths of only a few pixels: detecting these features requires more specialised approaches (Zhang et al., 2023). In this context, deep learning is a desirable and suitable approach to our classification problem.

The training data for our U-net consists of semi-automatically produced maps of surface water, enhancing traditional Normalised Difference Water Index (NDWI) maps with previously published post-processing techniques (Yang et al., 2019; Zhang et al., 2023) to extract high-frequency

crevasse and stream features. This process produces precise maps of water coverage, but production of these training data requires scene-specific manual tuning and is manually intensive, precluding its application at scale. This makes it a suitable candidate for training data production, with which we then train the U-net to replicate for large-scale application. We outline the full training and evaluation process in Supplementary Text 1.

We apply our water classification model to all Sentinel-2 scenes covering more than 40% of our study region that exist between April-September from 2016 and 2022. We download them from the Microsoft Planetary Computer, filtering to images that with <20% cloud cover and <80˚ solar zenith, resulting in a final total of a total of 862 scenes. Before classifying the images, we resample the data via cubic resampling to 10 m resolution polar stereographic north (EPSG:3413).

2.3 Time-Series Datasets

2.3.1 Identifying Contiguous Ponded Crevasse Fields

To present time-series of hydrological and dynamic behaviour specific to local crevasse fields, we defined individual contiguous crevasse field boundaries. We do this in two steps: the first is to identify a valid 'crevassed region' mask within which we reasonably interpret any water-filled pixel to be a water-filled crevasse (cf. a lake, stream, slush, etc). The second is to cluster these water-filled pixels into coherent 'ponded crevasse field' outlines within which we collate data on water coverage, average strain rate, and melt rate.

In the first step, we identify a region of potential crevasse fields as the intersection of three individual masks. The first mask is the GrIMP ice mask v1.2 (Howat, 2017) (Supplementary Fig. S2a). The second is derived from a pre-existing 200 m resolution map of crevasse fields (Chudley, 2022), which was generated from the ArcticDEM mosaic (Chudley et al., 2021). We identify any 200 m pixel >5% crevasse-filled as a crevasse field, and perform a morphological dilation-erosion operation (dilation of 500 m and erosion of 200 m) in order to generously include any misclassified margins (Supplementary Fig. S2b). Finally, we define a mask of all lakes by looping through all water masks in our dataset, morphologically eroding the mask by 50 m to eliminate rivers and crevasses, and subsequently morphologically dilate the mask by 150 m to obtain a buffered estimate of lake presence. We produce a lake mask where more than three images in the complete time-series stack are identified as a potential lake pixel (Supplementary Fig. S2c). We combine these masks to derive a final mask of potentially crevassed regions (Supplementary Fig. S2d).

In the second step, we aim to derive coherent and contiguous ponded crevasse fields from the dataset. We take the entire water-classified data stack, converting each water-filled pixel to a point with x and y spatial coordinates. We cluster these points into coherent regions using a Hierarchical Density-Based Spatial Clustering of Applications with Noise (HBDSCAN) approach (Campello et al., 2013; McInnes et al., 2017; McInnes & Healy, 2017). HBDSCAN is a robust unsupervised learning approach to detect dense clusters of varying sizes within a dataset, leaving sparse background points (i.e. noise) unclassified (the benefit of this can be seen in Fig. 1c). Due to

exponentially growing computational requirements as the number of points increases, we randomly sample 1% of water-classified points as input to the HBDSCAN algorithm. After points have been classified into spatially coherent clusters, we convert clustered points into individual (multi)polygons by buffering points by 200 m and removing small polygons beneath 0.2 km^2. Where clusters overlap, we divide the overlapping area evenly between the clusters. Finally, the automated clusters are manually quality assessed to ensure they represent real ponded crevasse fields. Out of 55 automated clusters, 48 were valid crevasse fields used for analysis: seven represented misclassified zones such as rivers or slush that were not successfully excluded by our masking process.

Based upon these crevasse field outlines (Fig. 1a), we extract time-varying records of ponded crevasse area, strain rates, and reanalysis melt data (Section 2.3.3 – 2.3.5). Although our full dataset covers 2016-2022, we focus exclusively on 2019 for detailed time-series analysis, as the year has a notably higher density of Sentinel-2 data coverage that allows for more precise determination of event timing. For each crevasse field, we identify a number of variables: whether the field drained in 2019; when the date of maximum water coverage was; and whether the maxima in water coverage was qualitatively observed to coincide with a maxima in melt rates.

2.3.2 Lakes and 'Empty' Crevasse Fields

To assess how unique the behaviours at ponded crevasse fields are, we further compare them to the evolution of ponded water, strain rates, and melt at (i) supraglacial lakes and (ii) 'empty' crevasse fields, which we define as regions of crevasse fields where water is not observed to pond through the observational dataset. The identification of lakes was described in Section 2.3.1: we again manually quality-assess the mask to remove misclassified regions (e.g. slush fields), detecting a total of 52 valid lakes from 68 polygons. A sample of 20 'empty' crevasse fields were manually outlined. The final ponded crevasse, lake, and empty crevasse outlines are shown in Supplementary Fig. S3.

2.3.3 Time-Series Water Data

We generate time-series records of water filling and drainage within crevasse fields and lakes from our CNN-classified Sentinel-2 scenes. Before extracting records, we first construct per-scene masks of invalid data, including NaN values and clouds. We estimate cloud cover as pixels that have a SWIR value > 0.14, following Williamson et al. (2018). We dilate this mask by 2 pixels (20 metres) to conservatively accommodate classification error. Following this, for every crevasse field/lake polygon, we loop through the dataset and record the area predicted to be water. If any pixels within the polygon are masked due to cloud or lack of data, the data point is rejected from further processing.

2.3.4 Time-Series Velocity and Strain Rate Data

We derive time-series logarithmic strain rates (Alley et al., 2018) from ITS_LIVE scene-pair ice velocity data (Gardner et al., 2024). We download all data between April-September 2016-22 derived from Sentinel-2 datasets and with a timestep of between 10 and 30 days. We eliminate

Landsat and Sentinel-1 records because qualitative analysis showed that Sentinel-2 scenes provide a product with much lower noise through the melt season, which is important for strain rate derivation. This was a similar motivation for filtering out timesteps beneath 10 days (anything greater than 30 days was considered of limited use for assessing strain rate evolution on the timescales of interest).

We define the surface strain rate tensor $\dot{\varepsilon}_{ij}$ in terms of the surface-parallel components of velocity u and v in Polar Stereographic North coordinate directions x and y, as

$$\dot{\varepsilon}_{ij} = \begin{bmatrix} \dfrac{\partial u}{\partial x} & \dfrac{1}{2}\left(\dfrac{\partial v}{\partial x} + \dfrac{\partial u}{\partial y}\right) \\ \dfrac{1}{2}\left(\dfrac{\partial v}{\partial x} + \dfrac{\partial u}{\partial y}\right) & \dfrac{\partial v}{\partial y} \end{bmatrix} = \begin{bmatrix} \dot{\varepsilon}_{xx} & \dot{\varepsilon}_{xy} \\ \dot{\varepsilon}_{xy} & \dot{\varepsilon}_{yy} \end{bmatrix}. \quad (1)$$

Strain rates are defined as positive in extension and negative in compression. We calculate logarithmic strain rates ($\dot{\varepsilon}_{xx}$, $\dot{\varepsilon}_{yy}$, and $\dot{\varepsilon}_{xy}$) following Alley et al. (2018). This approach calculates integrated deformation of ice parcels and is more resistant to errors than nominal strain rates in situations where large velocity gradients occur (such as at crevasse fields). The method requires a length scale value (r) to be determined as the radius from the pixel centre over which strain is calculated. Here, we set an r value of 500 m (effective length scale of 1000 m). Alley et al. (2018) originally proposed effective length scales between 3,000-6,000 m: this reflects their focus on large-scale viscous processes and longitudinal coupling on the order of ice thicknesses. Here instead, we are interested in smaller crevasse-scale processes, so desired an effective length scale ≤ 1 km. We tested with smaller r value of 250 m (effective length scale 500 m), but results did not visibly change.

We present strain rates in the form of first and second principal strain rates ($\dot{\varepsilon}_1$ and $\dot{\varepsilon}_2$), which we calculate as the highest (most extensional) and lowest (most compressive) eigenvalue of the strain rate tensor respectively, and the longitudinal (along-flow) strain rate ($\dot{\varepsilon}_{lon}$), which we calculate following Bindschadler et al. (1996) as

$$\dot{\varepsilon}_{lon} = \dot{\varepsilon}_{xx}\cos^2\alpha + 2\dot{\varepsilon}_{xy}\sin\alpha\cos\alpha + \dot{\varepsilon}_{yy}\sin^2\alpha. \quad (2)$$

where α is the direction of flow. Unlike previous analysis (Poinar & Andrews, 2021), we do not attempt to incorporate reported velocity uncertainty into our strain rate analysis. ITS_LIVE Sentinel-2 velocity fields provide only a single scene-wide value for uncertainty, which provides a much more conservative value that, in qualitative analysis, was an order of magnitude greater than the clear seasonal signals visible in the data.

To obtain time series for individual crevasse fields/lakes, we take the average value of velocity/strain rates within a polygon, so long as the polygon has full coverage.

2.3.5 Reanalysis Melt Data

We obtain melt rate data from RACMO2.3p2 at 1 km (statistically downscaled 5.5km) (Noël et al., 2019), based on ERA5 reanalyses. We present average daily melt rate within the crevasse field/lake boundaries, expressed in mm water equivalent (w.e.). Our choice to present average

daily melt rate rather than an integrated catchment runoff reflects the fact that individual crevasses within a field likely have a very small catchment and will not be receiving the total accumulated water from across the field. Hence, average daily melt rate provides a first-order indicator of the variation in daily meltwater available to any individual crevasse. Although is likely that this underestimates the total water received due to e.g. the melting of snow accumulated within crevasses (see Discussion), it remains useful as an indicator of drainage timing relative to key points within the ablation season such as the beginning of melt and the timing of maximum melt.

2.4 Linear Elastic Fracture Mechanics (LEFM) modelling

Following a LEFM approach to glacier crevasses (van der Veen, 1998), crevasses propagate to the depth within the ice (here approximated as a purely elastic material) at which the stress intensity factor at the fracture tip (K_I, Pa m$^{1/2}$) is equal to fracture toughness of ice (K_{Ic}). K_I can be divided into three components:

$$K_I = K_e + K_i + K_w, \tag{3}$$

where K_e is the contribution of the far-field resistive stress, K_i is the contribution of the ice overburden stress, and K_w is the contribution of the hydrostatic stress of water.

We use an LEFM model to derive fracture depths from Mode I fracture of individual surface crevasses. While the stress concentration at fracture tips will decrease as crevasse spacing decreases – and as such, treatments of individual crevasses will overestimate depths of closely-spaced crevasse fields – there is no convenient solution for such a case that accounts for the finite thickness of an ice body (van der Veen, 1998). Hence, the single fracture case is commonly used as a proxy (Clason et al., 2015; Gantayat et al., 2023), especially as it is unlikely that a perfectly uniform crevasse field of equal depth will exist in nature (Robin, 1974). We use the implementation of Lai et al. (2020), who use foundational equations derived from standard fracture mechanics handbooks (e.g. Tada et al., 2000). Following this approach, equation 3 can be expanded into its respective components as

$$K_I = \sqrt{\pi}\, R_{xx} d_s^{1/2} F(\tilde{d}_s) - \frac{2}{\sqrt{\pi}} \rho_i g d_s^{3/2} f(\tilde{d}_s) + \frac{2}{\sqrt{\pi}} \rho_w g d_s^{3/2} g(\tilde{d}_s, \tilde{d}_w), \tag{4}$$

(Lai et al., 2020 Eq. S5), where d_s is the depth of a crevasse, d_w is the depth of water within the crevasse, R_{xx} is the resistive stress, g is the gravitational constant (9.81 m s^{-1}), ρ_i and ρ_w are the densities of ice (917 kg m^{-3}) and water (1000 kg m^{-3}), respectively. Functions $F(\tilde{d}_s)$, $f(\tilde{d}_s)$, and $g(\tilde{d}_s, \tilde{d}_w)$ are dimensionless weight functions (given by Tada et al. (2000, p. 71) and presented in the Supplementary Text 2. $\tilde{d}_s \equiv \frac{d_s}{H}$, $\tilde{d}_w \equiv \frac{d_w}{d_s}$, and H is the ice thickness (here set to 1000 m). To assess water depths, we numerically solve eq. 4 for d_w where $K_I = K_{Ic}$. We set a minimum d_w value of 1 m to avoid numerical instability at low values of d_w. We set a nominal ice fracture toughness of 100 kPa m$^{1/2}$ as a broadly representative round value (Poinar et al., 2017).

Note that the values chosen for modelling parameters are, whilst plausible, deliberately illustrative rather than case-specific. We do not attempt to compare them directly with any observational

results in our study. Whilst LEFM is a standardised approach within the literature, more advanced numerical modelling (Jiménez & Duddu, 2018) shown that it is not the most suitable approach for predicting stress intensity factors where there is grounded ice with friction at the bed, as in this study. Our results should therefore be taken as predictors of broad behaviour under plausible conditions, rather than exact indicators of quantitative behavioural thresholds. In a comparative exercise, we also performed our modelling exercise under the alternative zero stress approximation: this produced similar results that did not change the conclusions of the exercise (Supplementary Text S3).

3. RESULTS

3.1 Drainage events

Our data indicate significant differences between the draining populations of ponded crevasses and supraglacial lakes. Of the 48 contiguous ponded crevasse fields we identified, 40 (83%) exhibited evidence of drainage in 2019. Similarly, of the 50 lakes, 20 (40%) exhibited evidence of drainage in 2019. On average, ponded crevasse fields begin to drain earlier than lakes. Ponded crevasses begin draining between 2019-05-05 and 2019-06-24 (mean: 2019-05-22), and lakes begin draining between 2019-05-10 and 2019-08-11 (mean: 2019-05-30), with a much longer tail (Supplementary Fig. S4a). The difference is statistically significant (p = 0.01). There was no statistically significant difference between the populations of ponded crevasses and lakes with regards to either the mean height of the features as identified from the ArcticDEM v4.1 mosaic (Porter et al., 2023), or the date of first appearance of melt in the RACMO dataset (Supplementary Fig. S4b-c). However, there was a significant (p = 0.01) difference in the 'background' strain rate as inferred from the ITS_LIVE velocity mosaic (Supplementary Fig. S4d), with lakes exhibiting a mean background longitudinal strain rate of -0.009 a^{-1} and ponded crevasses a rate of 0.014 a^{-1}.

3.2 Seasonal evolution

We further assessed the seasonal evolution of ponding, dynamics, and melt rate at our identified crevasses and lakes. Fig. 2 provides an example of the seasonal evolution of observed water cover, ice dynamics, and surface melt for a representative ponded crevasse field (identified in Fig. 1c). The crevasse field exhibits rapid growth in total water cover from the end of April/beginning of May, peaking in area on the 28th May. After this date, total water cover decays rapidly in an asymptotic fashion, losing ~50% of its area by 7th June (10 days) and continuing to decrease over the rest of the season. A visualisation of this in sequential Sentinel-2 imagery is included as Supplementary Animation 1. Parallel to this behaviour, we see a consistent increase in ice velocities through May, typical of seasonal behaviour at SKSG and understood to be caused by the onset of melt and subsequent evolution of subglacial hydrological networks (Howat et al., 2010). Longitudinal strain rates follow velocities, increasing throughout May as the crevasses fill. Whilst velocity and strain rates remain broadly constant for the rest of the season until the late-season termination of velocities, melt rates continue to increase and remain high following the drainage, suggesting that water is being routed elsewhere following the peak in water area.

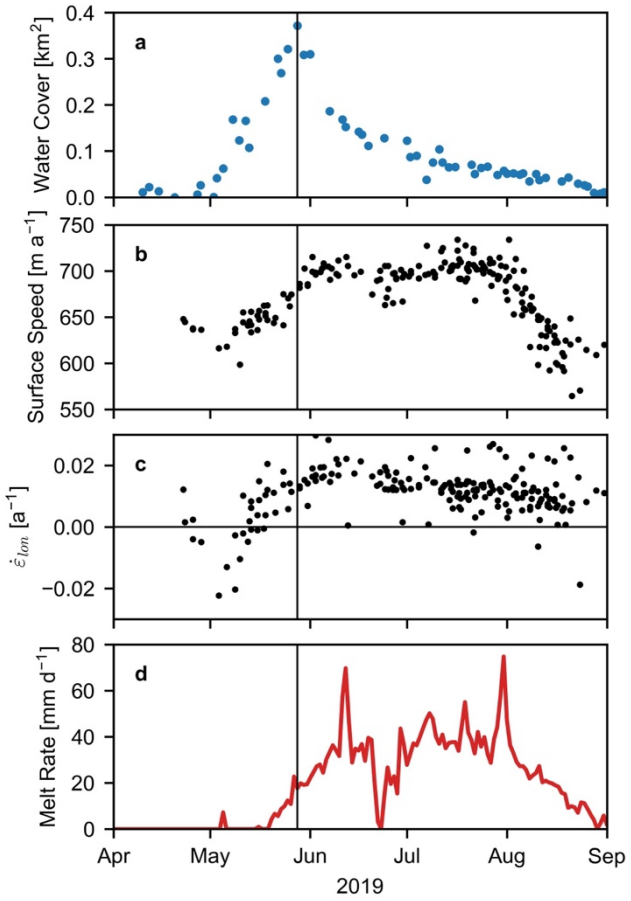

Figure 2. *Evolution of exemplar crevasse field (lower-right field in Fig. 1c) over the 2019 season. (a) Total water cover. (b) Mean ITS_LIVE ice surface speed. (c) Longitudinal strain rate, derived from ITS_LIVE velocity. (d) Mean RACMO daily melt rate. Vertical black line marks maximum observed water cover.*

To assess the extent to which the behaviour described above is quantitatively applicable across all drainage scenarios, we present aggregated data following Poinar & Andrews (2021) (Fig. 3). For crevasses and lakes that drain, we shift time series relative to the date of maximum water cover as a proxy for drainage date. For the 'empty' crevasses, we present time series as Julian Days. For each integer day, we take all measurements from all crevasses on that day (for velocity-derived data, this includes all data where the day falls between the date of the first and second scenes). We then generate a Gaussian KDE plot from the data to quantify a range of likely values on that day. The highest density is taken as the 'most likely' value, represented as black lines in Fig. 3.

Aggregated values show distinct seasonal patterns of the seasonal strain rate in ponded crevasse fields (Fig. 3a), lakes (Fig. 3b), and 'dry' crevasse fields (Fig. 3c). When assessing transient longitudinal strain rate, ponded crevasses (Fig. 3a) show a positive trend from compressive to extensional in the 50 days prior to drainage, reaching a maximum at 3 days prior to drainage (from -0.028 a^{-1} at t = -50 d to +0.019 a^{-1} at t = -3 d). A similar clear transition does not occur for supraglacial lake drainages (Fig. 3b), where strain rates generally fall within -0.01 a^{-1} to +0.01 a^{-1} throughout the entire season. Whilst there exists a slight negative deviation immediately prior to drainage (-0.014 at t =-4 d), this occurs during the period of sparsest observations and is not replicated in the Poinar & Andrews (2021) dataset (See Fig. 11 of Poinar & Andrews, 2021),

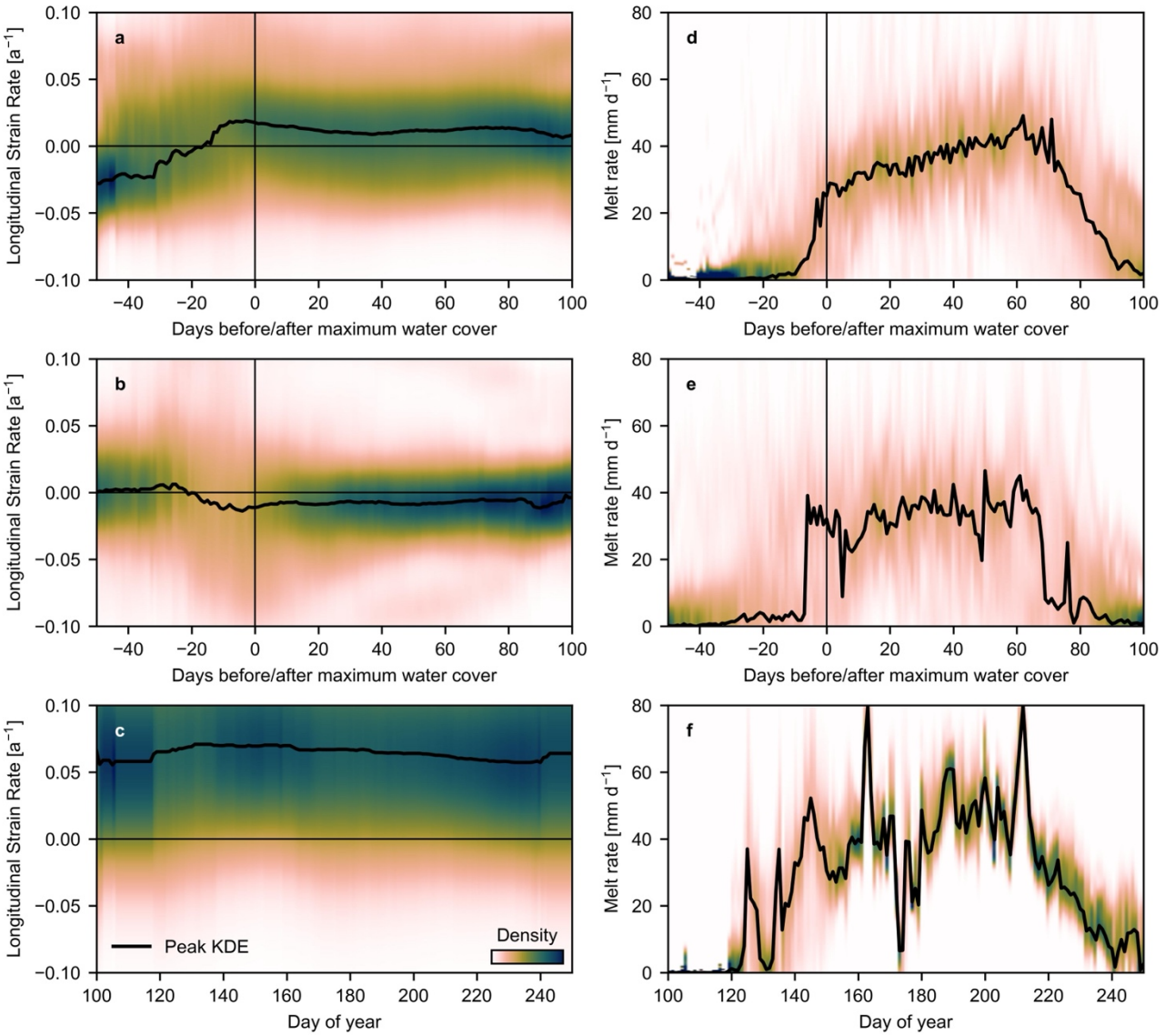

Figure 3. *Aggregated longitudinal strain rates (left column) and melt rate values (right column) for draining crevasses (top row), draining supraglacial lakes (middle row), and 'dry' crevasses that do not express surface water (bottom row). Colour scale represents Gaussian density estimates, and black line represents time series of highest Gaussian density estimate.*

suggesting it is not a reliable observation. Finally, at 'empty' non-ponding crevasses (Fig 3c), longitudinal strain rates are consistently highly extensional (>0.55 a^{-1}) through the summer season.

Aggregated RACMO melt rates indicates a weak relationship between the timing of drainage and melt rates. Drainage for both ponded crevasses (Fig. 3d) and lakes (Fig. 3e) show that drainages occur swiftly after the beginning of the melt season, but not at any peak in melt production. 3 (7.5%) of the draining crevasse fields did so in coincidence with a local peak in melt, whilst 2 (10%) of the draining lakes did so. This suggests that melt is a necessary, but not sufficient, condition for drainage in both scenarios.

3.3 LEFM Modelling

To quantitatively explore the effect of time-varying resistive stresses R_{xx} and water depths d_w on predicted fracture depth, we numerically solve LEFM equations for fracture depth d_s for a range of values of R_{xx} and d_w with fixed parameters H = 1000 m and K_{Ic} = 100 kPa m$^{1/2}$. We present nine

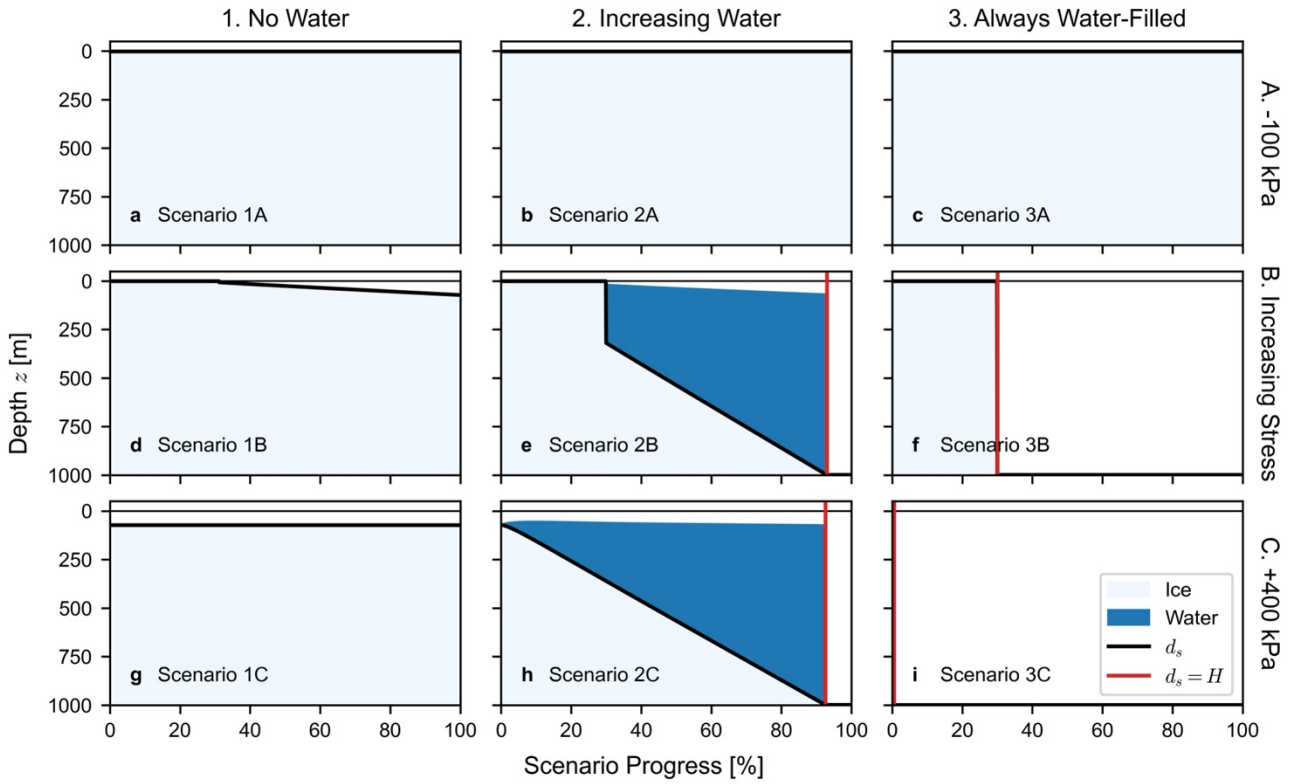

Figure 4. *LEFM modelling scenarios. (a-i) Time-series evolution of crevasse and water depths under R_{xx} forcing scenarios A-C (from top-bottom) and d_w forcing scenarios 1-3 (from left-right). Vertical red lines mark the timing of full-depth fracture ($d_s = H$). Panel represent scenarios: (a) 1A; (b) 2A; (c) 3A; (d) 1B; (e) 2B; (f) 3B; (g) 1C; (h) 2C; and (f) 3C. Scenarios are presented graphically in Supplementary Fig. S6.*

cases, each lasting 1000 timesteps, for all combinations of three prescribed scenarios of R_{xx} (scenarios A-C) and d_w (scenarios 1-3), respectively. In scenario A, R_{xx} remains low at -100 kPa for the full run; in B, it increases monotonically from -100 kPa to 400 kPa; and in C, it remains high at 400 kPa. Likewise, in scenario 1, d_w remains at 0 m (i.e. crevasses are always empty); in 2, d_w increases monotonically from 0 to 1000 m; and in 3, d_w remains at 1000 m (i.e. the crevasses are considered to always be filled with water). These scenarios are presented graphically in Supplementary Fig. S6.

The LEFM outputs (Fig. 4a-i) present distinct crevasse evolution outcomes. Where resistive stresses remain low (Fig. 4a-c), no crevasses will form as crevasse formation requires that the far-field stress contribution exceeds the ice fracture toughness ($K_e > K_{Ic}$), as when no crevasses exist ($d_w = 0$), K_i and K_w must be zero. When no water is present in crevasses, depths are limited (Fig. 4a,d,g), reaching no greater than 71.3 m at the maximum R_{xx} of 400 kPa. Only when water is present (and capable of filling most of the crevasse) are crevasses able to penetrate the full ice-sheet thickness to the bed. For the scenario 2B (Fig. 4e), this full-depth fracture occurs at $R_{xx} =$ 365 kPa, $d_w =$ 930 m, and scenario 2C (Fig. 4h) at $R_{xx} =$ 400 kPa, $d_w =$ 426 kPa. Under d_w scenario 3, where water is always able to fill the crevasse completely, full-depth hydrofracture is able to occur instantaneously upon the formation of a fracture (Fig. 4f,i). Fig 4f shows that under these conditions, when R_{xx} is variable and trending towards tensile stresses, it is the point at which $K_e > K_{Ic}$ that determines the timing of crevasse drainage. This is further emphasized when visualizing predicted d_w depths under the full range of R_{xx} and d_w values (Fig. 5), where the 'cliff

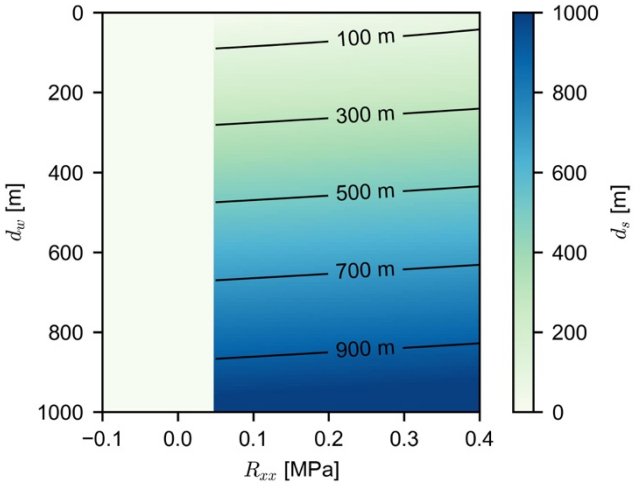

Figure 5. *Predicted crevasse depths under the full range of R_{xx} and d_w values considered, illustrating the 'cliff edge' of crevasse formation at the critical R_{xx} value.*

edge' is visible at the $K_e > K_{Ic}$ value. Hence, even though it is water availability that determines the ability of a crevasse to undergo full-depth hydrofracture, under scenarios where water is abundant and R_{xx} is approaching the critical fracture threshold value, the exact timing of drainage will be controlled by time-evolving ice dynamics.

4. DISCUSSION

4.1 Seasonal controls on ponded crevasse drainage

The data presented here indicate a strong relationship between crevasse drainage and ice dynamics, both in a spatial context and for time-evolving behaviour of ponded crevasses. As established in previous work (Chudley et al., 2021), ponded crevasses are preferentially likely to appear in zones of compression relative to unponded 'empty' crevasses. A reasonable expectation held in the wider literature (e.g. Poinar & Andrews, 2021) is that the first principal direction of stress should display a stronger control on behaviour than the flow-aligned longitudinal direction examined here. Replicating our analysis for the principal strain rates ($\dot{\varepsilon}_1$ and $\dot{\varepsilon}_2$) shows a broadly similar pattern of behaviour (Supplementary Fig. S5), but qualitatively weaker than for longitudinal strain rates. Additionally, only the longitudinal direction captures the transition from compressive to extensional strain rates, which has been suggested to be important in previous work (Chudley et al., 2021). Any individual direction of observed strain rate is unlikely to be perfectly predictive of the causal stresses leading to hydrofracture in the real environment, due the complex and multimodal nature of fracture (Grinsted et al., 2024; Reynolds et al., 2025). However, in this particular context, we consider it likely that compressive water-filled crevasses have advected out of the stress regime that formed them, weakening the connection between the local first principal strain rate and the 'real' multimodal stress leading to hydrofracture. Instead, flow-aligned longitudinal strain rate may represent a simpler link to a crevasse-orthogonal direction approximating Mode I fracture.

The good agreement between the transition to extensional strain rates and the subsequent onset of crevasse drainage (Fig. 3a) suggests that seasonal speed-ups and associated increases in extensional stress at the ice surface (cf Figs. 2b-c) play an important role in triggering full-depth

hydrofracture, particularly in contrast to the weak relationship between crevasse drainage and the daily melt rate (Fig. 3d). Seasonal speed-ups at Greenlandic outlets are commonly considered to be a function of changes: (i) at the ice-ocean-boundary – for example, mélange break-up reducing buttressing – and (ii) in subglacial hydrology, including a melt-induced 'spring event' of seasonal acceleration that is a common feature across both land-terminating (Bartholomew et al., 2010) and marine-terminating (Moon et al., 2014) sectors of the GrIS. At SKSG, late-season slowdowns in speed are attributed a particular sensitivity to shutdowns in the subglacial hydrological system relative to the average marine-terminating outlet (Cook et al., 2020; Howat et al., 2010).

We suggest that a causal link between extensional strain rates and the onset of crevasse drainage arises from peaks in the crevasse-orthogonal stress (R_{xx} within the LEFM framework). However, this relationship contrasts with traditional understandings of hydrofracture, whereby it is the depth of the water column within the crevasse that is the most important variable in driving crevasse propagation, and varying the resistive stresses has a much smaller effect (van der Veen, 1998, 2007; Weertman, 1973). Our LEFM modelling experiments (Section 3.3) provide an insight into this context. Unsurprisingly, the results of our experiments support the principle that crevasses cannot drain by tensile stresses alone (Fig 4a,d,g), and that crevasses must necessarily be (nearly) filled with water to propagate fully to the bed (Fig 4e,f,h,i). However, our experiments additionally include the consideration of time-varying resistive stress, whereas previously experiments have considered only fixed R_{xx} values, even where multiple options for R_{xx} have been considered (e.g. Krawczynski et al., 2009). These show that, if meltwater is abundant (i.e. sufficient water exists that the crevasse can always be water-filled), the critical factor in determining the timing of crevasse drainage is the point at which the far-field resistive stress contribution exceeds the ice strength ($K_e > K_{Ic}$) and thus fractures can begin to open. This is governed exclusively by the time-varying value of R_{xx}. Once open, the fractures can propagate to the bed by water-filling alone.

There are two problems with relating our LEFM inferences to the observational record. First, LEFM assumes that fractures are closed under compressive or near-neutral stresses, given the model considers only elastic responses (assumed to be effectively instantaneous) rather than any viscous deformation. However, the ponded crevasses we observe already exist and appear significant in size, on the order of 10-100 m in width and 100-1000 m in length, and even the surface expression visible in metre-scale-resolution elevation datasets can be 10-100 m deep (Chudley et al., 2025; Enderlin & Bartholomaus, 2020). Second, it requires the assumption that crevasses have access to abundant meltwater such that they can always be water-filled, regardless of the depth or volume of the crevasse. However, UAV observations suggest that these ponded crevasses are hydraulically isolated with small catchments, limiting access to runoff (Chudley et al., 2021).

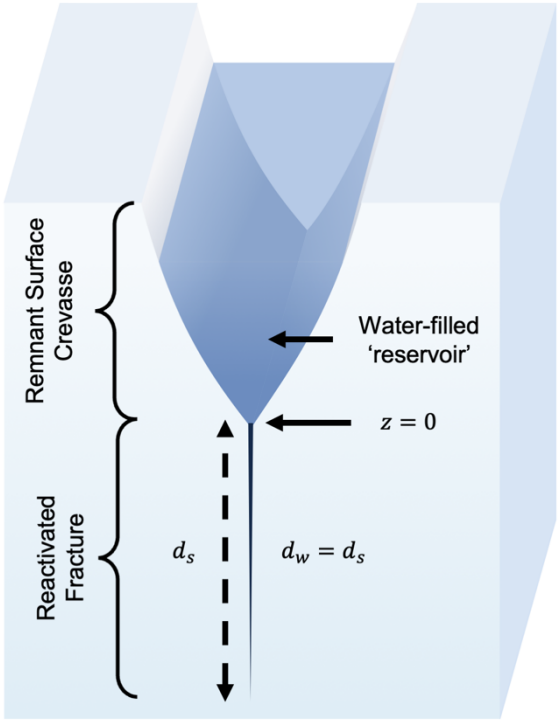

Fig 6. *Schematic conceptualisation of a fracture underlying a water 'reservoir' in the remnant of a viscously closed surface feature. Note that the origin of z (the depth relative to the top of the fracture) is the bottom of the reservoir, rather than the ice surface.*

We suggest that these problems can be resolved by conceptualising surface crevasses in compressive regimes as viscously closed features with a V-shaped remnant surface expression, following Poinar's (2020) description of 'water-filled ditches' (Fig. 6). Here, remnant crevasse fields can fill with snow overwinter, producing a significant reservoir of water early in the melt season. The relict fracture, healed either via viscous closure or via refreezing (Hubbard et al., 2021), remains at the base of the ditch. The fracture remains susceptible to reactivation from infilling water, as has been observed to trigger the drainage of supraglacial lakes (Chudley et al., 2019; Humbert et al., 2025). The reservoir overlying this fracture cannot influence the stress intensity factor, as being substantially wider than the fracture itself, the overburden pressure is influencing both water and ice overburden (K_w and K_i) equally (see Law, 2025). Upon initial (re)opening of the fracture in response to seasonally increasing tensile stresses, water from the overlying reservoir can enter the fracture, providing an abundant and continuous supply of meltwater to promote immediate (in model terms) full-depth hydrofracture, analogous to supraglacial lake drainage.

Simple calculations show that snowfall present in relict crevasses at the beginning of the season could provide the vast majority of water necessary to encourage full-depth propagation. Nominal crevasse widths (and thus requisite reservoir volumes) are relatively low: with 0.1 – 1.0 m being a reasonable range of crevasse widths to efficiently drain lakes in LEFM modelling (Krawczynski et al., 2009), matching the 0.4 m observed by Doyle *et al.* (2013). If we assume a simplified semicircular surface relict feature of 50 m diameter that begins the season filled with compacted snow of 400 kg m^{-3}, an along-flow profile would contain ~390 m^2 of water once fully melted. This is enough to completely fill a 0.4 m wide fracture ~980 m deep – sufficient to induce full-depth fracture in a 1 km thick ice sheet without requiring additional water contribution from non-local

runoff (although in practice, not all snow will melt and accumulated runoff will form some proportion of meltwater). With regional daily snowfall trends on the order of 1 mm/day during the accumulation season (Gallagher et al., 2022), directly accumulated snow alone is insufficient to fill large crevasses. However, in-situ observations at SKSG suggest that even large (>10 m diameter) crevasses can begin the melt season filled with snow (Figure S7), and Alpine observations indicate that wind-blown snow is a critical component of crevasse snow-filling (Ravanel et al., 2022). Strong katabatic winds and dry winter snow likely provide a highly conducive environment for snow redistribution from over large distances (Li & Pomeroy, 1997), although studies quantifying these processes over the Greenland Ice Sheet are sparse (Zuhr et al., 2021).

One final consideration is the ability for ponded crevasses to exhibit repeated fill and drainage behaviour throughout the year, as noted by Cavanagh et al. (2017). Although this is not common in our dataset (only 4 crevasse fields / 10% of the total exhibit repeat filling/drainages in 2019), the literature suggests that this appears to be relatively unique to ponded crevasses fields and not supraglacial lakes. We suggest that multiple drainages likely occur because – given the small catchment available for meltwater accumulation and delivery to individual crevasses – the ongoing rate of runoff into a fracture is insufficient to maintain an open moulin through thermomechanical erosion. Instead, the fracture can close visco-elastically, refill with water given abundant peak melt rates (Fig. 3d), and then drain again if conditions are sufficient.

4.2 Differences between ponded crevasses and other surface drainage features

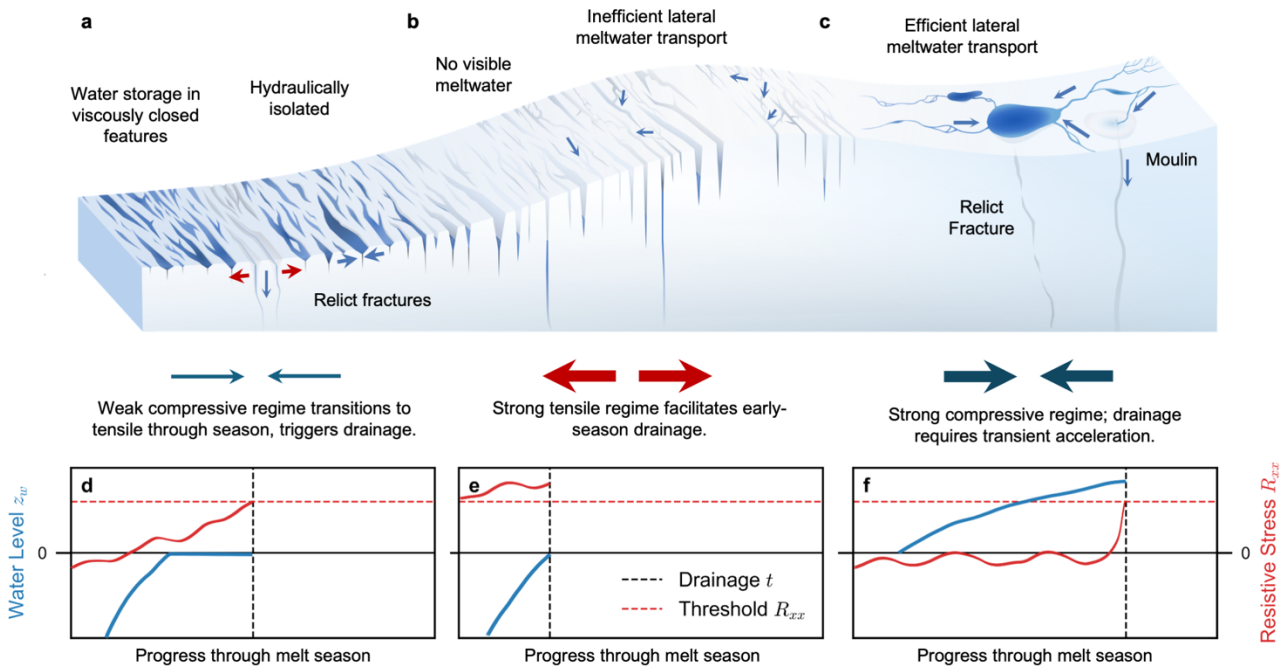

Figure 7. *(a-c) Conceptual framework showing hydrological surface features across the ablation zone of a fast-flowing outlet glacier, and (d-e) proposed evolution of water levels relative to the ice surface (z_w, blue) and resistive stresses (R_{xx}, red) until drainage occurs (dashed vertical line) at these locations. (a, d) At ponded crevasses, being water-filled is a necessary but not sufficient condition for hydrofracture: R_{xx} values must reach a critical threshold for fracture formation before drainage can occur. (b, e) At empty crevasses, resistive stresses are sufficient for fracture formation – crevasses can drain early in the season upon sufficient meltwater accumulation. (c, f) At lakes, R_{xx} remains low throughout the season: short-term transient accelerations are necessary to reach the threshold for fracture initiation.*

4.2.1 Lakes

Our proposal that ponded crevasses drain due to a secular seasonal trend towards tensile stresses differs significantly from hypotheses relating to supraglacial lake drainage. At supraglacial lake sites, which are preferentially located in compressive regimes (Poinar & Andrews, 2021), initial hydrofracture is not preceded by increases in stress state on the scale of weeks, shown by Poinar & Andrews (2021) as well as our data (Fig. 3b). Instead, reaching sufficient tensile stresses to drain lakes requires short-term (~hours-days) transient precursor events (Christoffersen et al., 2018; Hoffman et al., 2018; Poinar & Andrews, 2021; Stevens et al., 2015, 2024). In other circumstances, relict fractures from preceding years can be reopened in subsequent years along planes of weakness (Chudley et al., 2019; Humbert et al., 2025). Observations suggest that the stress intensity factor required to reactivate fractures is not as great as required to initiate new fractures: drainage in these scenarios can occur either without a precursory dynamic event (Chudley et al., 2019) or at lower lake volumes (Humbert et al., 2025). We suggest the mechanical difference between lake and ponded crevasse drainage is related to the different background stress regimes. Whilst lakes may exist in a compressive environment through the entire season (Fig. 3b) and require transient events to initiate fracture, ponded crevasses exist in an intermediate context, switching from compressive to extensional within the same season (Fig. 3a), a transition that facilitates full-depth hydrofracture.

A further difference between lake and crevasse field drainage is the anticipated rate of water delivery to the bed. Supraglacial lake drainages can drain completely in a matter of hours (Doyle et al., 2013; Stevens et al., 2015), which is reflected in remote sensing classification thresholds. For instance, rapid drainages are classified as lakes exhibiting >80% volume loss in ≤4 days at SKSG by Williamson *et al.* (2018). This rapid loss in water cover is replicated in our lake drainage observations (Fig. S8). Conversely, in our contiguous crevasse field datasets, the loss in significant water-filled crevasse area instead occurs over days or weeks (Fig. 2). This reflects the fact that drainage does not occur simultaneously across an entire ponded crevasse field, but as a series of sequential drainages of individual crevasses (Supplementary Animation S1). These respond to a single overriding control (increasingly tensile resistive stress) but are subject to stochastic variation based upon secondary factors (e.g. catchment and meltwater availability, stress field variability across crevassed regions, variations in the stress intensity factor). This variation likely explains why we observe strain rates to peak in the days before water cover (Fig. 3a) – fractures may begin draining prior to this date, although only once drainage rates exceed meltwater filling rates will total water cover begin to decrease.

4.2.2 'Empty' crevasses

In crevasse fields where no ponding is observed, strain rates remain tensile and high in magnitude through the entire season (Fig. 3c), suggesting highly extensional stresses may explain this behaviour. One previous hypothesis is that crevasses in these regions are not hydraulically isolated (Chudley et al., 2021) and no ponding is expressed because meltwater is transferred laterally through englacial fracture networks to pre-existing moulins. Whilst pre-existing fracture

networks are largely confined to temperate glaciers (Fountain et al., 2005) and cannot explain full-depth water transfer, there is direct (radar evidence: Kendrick et al., 2018) and indirect (near-surface cryo-hydologic warming: Hubbard et al., 2021; Law et al., 2021) of substanial water systems occurring in the upper 0-100 m of crevasse fields at SKSG. Given significant evidence of cross-cutting crevasses in highly extensional regimes (Chudley et al., 2021), it may be reasonable for this englacial water to be able to be routed laterally to pre-existing moulins, resulting in substantially slower rates of meltwater delivery to the bed than via full-depth hydofracture, or through moulins fed by surface streams (Colgan et al., 2011; McGrath et al., 2011).

A second hypothesis is that no water is observed in 'empty' crevasses because they drain near-instantaneously to the bed upon the commencement of the melt season (forcing scenario 3C in fig. 4j). This mechanism could explain how the earliest meltwater of the season can arrive at the bed. Ponded crevasses drain as a consequence, rather than a cause, of seasonal acceleration (Fig. 3a), yet seasonal accelerations at SKSG (and many other marine-terminating outlets) are well-understood to be due to the onset of melt and reductions in effective pressure (Moon et al., 2014; Vijay et al., 2019). The ability for crevasses in tensile regimes to drain to the bed without the requirement for any seasonal acceleration may provide the initial route through which hydrologically-forced acceleration begins (see also Khan et al., 2025). However, 'active' crevasses opening in tensile regimes will lack a significant reservoir of water to initiate hydrofracture, in contrast to the 'water-filled ditches' (Poinar, 2020) overlying relict fractures in compressive regimes. This may instead be compensated by the lateral englacial water transport through open fracture networks (Benn et al., 2009), feeding initial hydrofractures and subsequent moulins. The precise mechanism is challenging to infer from remote sensing studies alone: field observations, such as airborne ice-penetrating radar, may be able to provide further insights into the nature of the hydrological networks within surface crevasse fields.

4.3 Parameterising crevasse fields in models

Spatio-temporal variability in meltwater inputs to the bed has been shown to affect the configuration of the subglacial drainage system (Andrews et al., 2014; Banwell et al., 2016; Scholzen et al., 2021), but properly representing this behaviour in modelling studies is limited by our ability to parameterise surface-to-bed meltwater routing. Within the range of studies that have included surface-to-bed routing representation in models (e.g. Clason et al., 2012, 2014; Gowan et al., 2023; Koziol & Arnold, 2018), even fewer have considered crevasse fields explicitly. A common initial approach is to approximate the distribution of crevasses based upon a threshold stress value (Clason et al., 2012, 2015; Gantayat et al., 2023; Koziol et al., 2017). Following this, two common choices are made. The first is to allow runoff generated over crevasse fields to reach the bed immediately and directly upon formation, rather than in any discrete inputs (Koziol et al., 2017; Sommers et al., 2024). This approximates a hydraulically transmissive crevasse field that readily transports meltwater to the bed. The second is to allow meltwater to pond and drain following an LEFM framework, often using the background stress as a fixed R_{xx} value (Clason et al., 2015; Everett et al., 2016; Gantayat et al., 2023). These two approaches result in considerably different

patterns of meltwater delivery (spatio-temporally uniform vs discrete) which are understood to have distinct consequences for the subglacial hydrological system (Banwell et al., 2016; Schoof, 2010).

Our observations provide new insight into ways to better represent crevasse drainage processes within surface-to-bed routing models. The first is the careful consideration of which stress representation to use as a proxy for R_{xx}. Our baseline here is the Von Mises failure criterion, which is the most common choice of representative stress in surface-to-bed routing models (Clason et al., 2012, 2015; Gantayat et al., 2023). The criterion is established as a good approximation for ice failure (Vaughan, 1993), but it may not be similarly appropriate for the case of ponded crevasse fields. Von Mises thresholds predict zones of active failure, whereas ponded crevasse fields represent relict crevasse fields that have advected into compressive regimes (Fig. 7; Poinar, 2020). Second, because von Mises stress is direction-insensitive (treating tensile and compressive stresses of the same magnitude identically), it is not always a suitable proxy for processes where the sign of stress matters (Grinsted et al., 2024), as suggested by our time-series strain rate analysis (Fig. 3). Ultimately any individual choice of proxy will have weaknesses in a simple parameterisation, as crevasses in nature will be a function of complex multi-modal stresses. However, when considering Mode-I fracture (which LEFM approaches implicitly assume), using the first principal (tensile) Cauchy stress or longitudinal stress is likely more appropriate (Reynolds et al., 2024).

The second recommendation is to include time-varying stresses in surface-to-bed routing models. Whilst static background stress derived from annual velocity fields appear to be useful in predicting broad behaviours (Chudley et al., 2021; Poinar & Andrews, 2021), the exact timing of drainage of ponded crevasse fields requires knowledge of seasonally-varying stress (Fig. 3a). Everett et al. (2016) report that their LEFM model predictions of drainage date are poorer for water-filled crevasses than for supraglacial lakes, which they conclude is due to variation in subglacial hydrological potential. An additional factor may be that the seasonal evolution of stresses are important for crevasse drainage in a way that they are not for supraglacial lake drainage. To force a regional surface-to-bed routing model with time-varying stresses would require representative stress values, generated either from observations or modelling. Observationally, continuous records of stress fields could be generated from remotely-sensed velocity records. This would require methods of statistically generating infilled data – for example, Bayesian methods such as Gaussian process regression (Guillet et al., 2025). A modelling approach would require a coupled hydrology-dynamic model, which a long-term desirable goal that would be able to account for coupled feedbacks between the meltwater drainage and basal sliding (Gantayat et al., 2023).

5. SUMMARY AND CONCLUSIONS

Our work has presented the first assessment of the interaction between seasonal ice dynamics and crevasse hydrology at a fast-flowing outlet glacier. Combining Earth observation data with mechanical insights from LEFM, we conclude that seasonal ice dynamics exert a dominant control over when ponded crevasse fields drain at fast-flowing Greenlandic outlets. Regions of crevasse ponding are characterised by topographically distinct relict surface ‘ditches’, formed from the

viscous closure of active crevasse fields as they advect into compressive or near-neutral background stresses. These features allow for large reservoirs of water to be generated rapidly in the melt season despite small catchment areas, likely from the melt of overwinter snowfill. As the melt season progresses and the ice sheet accelerates, increasingly tensile stresses eventually reach a sufficient threshold to trigger new fracture underlying the reservoirs. Abundant meltwater provided from the overlying reservoirs allows for rapid full-depth hydrofracture to the ice sheet bed. These findings support a new conceptual framework of meltwater drainage at fast-flowing glaciers, distinct from established mechanisms of drainage at supraglacial lakes (which likely are triggered by short-term dynamic accelerations), and likely distinct from processes occurring within 'empty' crevasse fields where crevasses are not observed to fill with water. Crevasse drainage is thought to transfer at least half of all water to the bed of the Greenland Ice Sheet, and the influence of ice dynamics on crevasse hydrofracture is likely important across wider regions of the cryosphere, such as Antarctic ice shelves, marine-terminating ice caps, and surging glaciers. The insights outlined here provide the groundwork to properly parameterise crevasse drainage behaviours into numerical models and understand their influence on the seasonal and long-term evolution of ice sheet and glacier processes.

DATA AVAILABILITY STATEMENT

Data and Jupyter Notebooks necessary to reproduce the study are available at https://doi.org/10.5281/zenodo.17287272 (Chudley, 2025). Sentinel-2 data were downloaded from the Microsoft Planetary Computer. ITS_LIVE velocity data are available from Gardner et al. (2024). The GrIMP ice mask is available from Howat et al. (2017). The ArcticDEM-derived crevasse mask is available from Chudley (2022). RACMO2.3p2 data are available from the authors of Noël et al. (2019). The ArcticDEM v4.1 mosaic was downloaded using *pdemtools* (Chudley & Howat, 2024). The TensorFlow model, alongside supporting functions and explanatory Jupyter Notebook for water classification, will be made available on Github/Zenodo upon publication.

ACKNOWLEDGEMENTS

TRC received funding from a Leverhulme Trust Early Career Fellowship (ECF-2022-589). JML received funding from a United Kingdom Research and Innovation (UKRI) Future Leaders Fellowship (MR/X02346X/1). We are grateful to colleagues for fruitful discussions that fed into the work: to Kristin Poinar on strain rate analysis and water-filled ditches; to Jonny Kingslake on the application of overlying water to linear elastic fracture mechanics; and to Patrice Carbonneau and Wei Ji Leong on development of the deep learning architecture. Poul Christoffersen provided the Fig. S7 photograph. This work has used Durham University's NVIDIA CUDA Centre (NCC) cluster. NCC has been purchased through Durham University's strategic investment funds and is installed and maintained by the Department of Computer Science.

AUTHOR CONTRIBUTIONS

Conceptualisation: TRC, CRS, JML, CCC
Methodology: TRC, TW, RL, JLD

Formal analysis: TRC

Visualisation: TRC, HEW

Funding Acquisition: TRC, CRS, JML

Writing – Original Draft: TRC

Writing – Review & Editing: TRC, CRS, JML, TW, RL, CCC, HEW, JLD

CONFLICT OF INTEREST DISCLOSURE

The authors declare no conflicts of interest relevant to this study.

REFERENCES

Alley, K. E., Scambos, T. A., Anderson, R. S., Rajaram, H., Pope, A., & Haran, T. M. (2018). Continent-wide estimates of Antarctic strain rates from Landsat 8-derived velocity grids. *Journal of Glaciology*, *64*(244), 321–332. https://doi.org/10.1017/jog.2018.23

Andrews, L. C., Catania, G. A., Hoffman, M. J., Gulley, J. D., Lüthi, M. P., Ryser, C., et al. (2014). Direct observations of evolving subglacial drainage beneath the Greenland Ice Sheet. *Nature*, *514*(7520), 80–83. https://doi.org/10.1038/nature13796

Banwell, A., Hewitt, I., Willis, I., & Arnold, N. (2016). Moulin density controls drainage development beneath the Greenland ice sheet. *Journal of Geophysical Research: Earth Surface*, 2015JF003801. https://doi.org/10.1002/2015JF003801

Bartholomew, I., Nienow, P., Mair, D., Hubbard, A., King, M. A., & Sole, A. (2010). Seasonal evolution of subglacial drainage and acceleration in a Greenland outlet glacier. *Nature Geoscience*, *3*(6), 408–411.

Bell, R. E., Tinto, K., Das, I., Wolovick, M., Chu, W., Creyts, T. T., et al. (2014). Deformation, warming and softening of Greenland's ice by refreezing meltwater. *Nature Geoscience*, *7*(7), 497–502. https://doi.org/10.1038/ngeo2179

Benn, D., Gulley, J., Luckman, A., Adamek, A., & Glowacki, P. S. (2009). Englacial drainage systems formed by hydrologically driven crevasse propagation. *Journal of Glaciology*, *55*(191), 513–523. https://doi.org/10.3189/002214309788816669

Bindschadler, R., Vornberger, P., Blankenship, D., Scambos, T., & Jacobel, R. (1996). Surface velocity and mass balance of Ice Streams D and E, West Antarctica. *Journal of Glaciology*, *42*(142), 461–475. https://doi.org/10.3189/S0022143000003452

Campello, R. J. G. B., Moulavi, D., & Sander, J. (2013). Density-Based Clustering Based on Hierarchical Density Estimates. In J. Pei, V. S. Tseng, L. Cao, H. Motoda, & G. Xu (Eds.), *Advances in Knowledge Discovery and Data Mining* (pp. 160–172). Berlin, Heidelberg: Springer. https://doi.org/10.1007/978-3-642-37456-2_14

Cavanagh, J. P., Lampkin, D. J., & Moon, T. (2017). Seasonal Variability in Regional Ice Flow Due to Meltwater Injection Into the Shear Margins of Jakobshavn Isbræ. *Journal of Geophysical Research: Earth Surface*, *122*(12), 2488–2505. https://doi.org/10.1002/2016JF004187

Christoffersen, P., Bougamont, M., Hubbard, A., Doyle, S. H., Grigsby, S., & Pettersson, R. (2018). Cascading lake drainage on the Greenland Ice Sheet triggered by tensile shock and fracture. *Nature Communications*, *9*(1), 1064. https://doi.org/10.1038/s41467-018-03420-8

Chudley, T. R. (2022). Greenland Ice Sheet crevasse map from ArcticDEM [Data set]. Zenodo. https://doi.org/10.5281/zenodo.6779087

Chudley, T. R. (2025, October 7). Data supporting "Seasonal ice dynamics control the timing of crevasse drainage at a fast-flowing outlet glacier." Zenodo. https://doi.org/10.5281/zenodo.17287273

Chudley, T. R., & Howat, I. M. (2024). pDEMtools: conveniently search, download, and process ArcticDEM and REMA products. *Journal of Open Source Software*, *9*(102), 7149. https://doi.org/10.21105/joss.07149

Chudley, T. R., Christoffersen, P., Doyle, S. H., Bougamont, M., Schoonman, C. M., Hubbard, B., & James, M. R. (2019). Supraglacial lake drainage at a fast-flowing Greenlandic outlet glacier. *Proceedings of the National Academy of Sciences*. https://doi.org/10.1073/pnas.1913685116

Chudley, T. R., Christoffersen, P., Doyle, S. H., Dowling, T. P. F., Law, R., Schoonman, C. M., et al. (2021). Controls on Water Storage and Drainage in Crevasses on the Greenland Ice Sheet. *Journal of Geophysical Research: Earth Surface*, *126*(9), e2021JF006287. https://doi.org/10.1029/2021JF006287

Chudley, T. R., Howat, I. M., King, M. D., & MacKie, E. J. (2025). Increased crevassing across accelerating Greenland Ice Sheet margins. *Nature Geoscience*, *18*(2), 148–153. https://doi.org/10.1038/s41561-024-01636-6

Clason, C. C., Mair, D. W. F., Burgess, D. O., & Nienow, P. W. (2012). Modelling the delivery of supraglacial meltwater to the ice/bed interface: application to southwest Devon Ice Cap, Nunavut, Canada. *Journal of Glaciology*, *58*(208), 361–374. https://doi.org/10.3189/2012JoG11J129

Clason, C. C., Applegate, P. J., & Holmlund, P. (2014). Modelling Late Weichselian evolution of the Eurasian ice sheets forced by surface meltwater-enhanced basal sliding. *Journal of Glaciology*, *60*(219), 29–40. https://doi.org/10.3189/2014JoG13J037

Clason, C. C., Mair, D. W. F., Nienow, P. W., Bartholomew, I. D., Sole, A., Palmer, S., & Schwanghart, W. (2015). Modelling the transfer of supraglacial meltwater to the bed of Leverett Glacier, Southwest Greenland. *The Cryosphere*, *9*(1), 123–138. https://doi.org/10.5194/tc-9-123-2015

Colgan, W., Steffen, K., McLamb, W. S., Abdalati, W., Rajaram, H., Motyka, R., et al. (2011). An increase in crevasse extent, West Greenland: Hydrologic implications. *Geophysical Research Letters*, *38*(18). https://doi.org/10.1029/2011GL048491

Colgan, W., Sommers, A., Rajaram, H., Abdalati, W., & Frahm, J. (2015). Considering thermal-viscous collapse of the Greenland ice sheet. *Earth's Future*, *3*(7), 252–267. https://doi.org/10.1002/2015EF000301

Cook, S. J., Christoffersen, P., Todd, J., Slater, D., & Chauché, N. (2020). Coupled modelling of subglacial hydrology and calving-front melting at Store Glacier, West Greenland. *The Cryosphere*, *14*(3), 905–924. https://doi.org/10.5194/tc-14-905-2020

Cook, S. J., Christoffersen, P., & Todd, J. (2022). A fully-coupled 3D model of a large Greenlandic outlet glacier with evolving subglacial hydrology, frontal plume melting and calving. *Journal of Glaciology*, *68*(269), 486–502. https://doi.org/10.1017/jog.2021.109

Cowton, T., Slater, D., Sole, A., Goldberg, D., & Nienow, P. (2015). Modeling the impact of glacial runoff on fjord circulation and submarine melt rate using a new subgrid-scale parameterization for glacial plumes. *Journal of Geophysical Research: Oceans*, *120*(2), 796–812. https://doi.org/10.1002/2014JC010324

Doyle, S. H., Hubbard, A. L., Dow, C. F., Jones, G. A., Fitzpatrick, A., Gusmeroli, A., et al. (2013). Ice tectonic deformation during the rapid in situ drainage of a supraglacial lake on the Greenland Ice Sheet. *The Cryosphere*, *7*(1), 129–140. https://doi.org/10.5194/tc-7-129-2013

Doyle, S. H., Hubbard, B., Christoffersen, P., Young, T. J., Hofstede, C., Bougamont, M., et al. (2018). Physical Conditions of Fast Glacier Flow: 1. Measurements From Boreholes Drilled to the Bed of Store Glacier, West Greenland. *Journal of Geophysical Research: Earth Surface*. https://doi.org/10.1002/2017JF004529

Enderlin, E. M., & Bartholomaus, T. C. (2020). Sharp contrasts in observed and modeled crevasse patterns at Greenland's marine terminating glaciers. *The Cryosphere*, *14*(11), 4121–4133. https://doi.org/10.5194/tc-14-4121-2020

Everett, A., Murray, T., Selmes, N., Rutt, I. C., Luckman, A., James, T. D., et al. (2016). Annual down-glacier drainage of lakes and water-filled crevasses at Helheim Glacier, southeast Greenland. *Journal of Geophysical Research: Earth Surface*, *121*(10), 1819–1833. https://doi.org/10.1002/2016JF003831

Fountain, A. G., Jacobel, R. W., Schlichting, R., & Jansson, P. (2005). Fractures as the main pathways of water flow in temperate glaciers. *Nature*, *433*(7026), 618–621. https://doi.org/10.1038/nature03296

Gallagher, M. R., Shupe, M. D., Chepfer, H., & L'Ecuyer, T. (2022). Relating snowfall observations to Greenland ice sheet mass changes: an atmospheric circulation perspective. *The Cryosphere*, *16*(2), 435–450. https://doi.org/10.5194/tc-16-435-2022

Gantayat, P., Banwell, A. F., Leeson, A. A., Lea, J. M., Petersen, D., Gourmelen, N., & Fettweis, X. (2023). A new model for supraglacial hydrology evolution and drainage for the Greenland Ice Sheet (SHED v1.0). *Geoscientific Model Development*, *16*(20), 5803–5823. https://doi.org/10.5194/gmd-16-5803-2023

Gardner, A., Fahnestock, M., Greene, C. A., Kennedy, J. H., Liukis, M., Lopez, L. A., & Scambos, T. (2024). MEASURES ITS_LIVE Regional Glacier and Ice Sheet Surface Velocities, Version 2 [Data set].

NASA National Snow and Ice Data Center Distributed Active Archive Center. https://doi.org/10.5067/JQ6337239C96

Gowan, E. J., Hinck, S., Niu, L., Clason, C., & Lohmann, G. (2023). The impact of spatially varying ice sheet basal conditions on sliding at glacial time scales. *Journal of Glaciology*, *69*(276), 1056–1070. https://doi.org/10.1017/jog.2022.125

Grinsted, A., Rathmann, N. M., Mottram, R., Solgaard, A. M., Mathiesen, J., & Hvidberg, C. S. (2024). Failure strength of glacier ice inferred from Greenland crevasses. *The Cryosphere*, *18*(4), 1947–1957. https://doi.org/10.5194/tc-18-1947-2024

Guillet, G., Benn, D. I., King, O., Shean, D., Mannerfelt, E. S., & Hugonnet, R. (2025). Global detection of glacier surges from surface velocities, elevation change and SAR backscatter data between 2000 and 2024: a test of surge mechanism theories. *Journal of Glaciology*, *71*, e88. https://doi.org/10.1017/jog.2025.10065

Hoffman, M. J., Perego, M., Andrews, L. C., Price, S. F., Neumann, T. A., Johnson, J. V., et al. (2018). Widespread Moulin Formation During Supraglacial Lake Drainages in Greenland. *Geophysical Research Letters*, *45*(2), 778–788. https://doi.org/10.1002/2017GL075659

Howat, I. M. (2017). MEaSUREs Greenland Ice Mapping Project (GIMP) Land Ice and Ocean Classification Mask, Version 1 [Data set]. NASA National Snow and Ice Data Center Distributed Active Archive Center. https://doi.org/10.5067/B8X58MQBFUPA

Howat, I. M., Box, J. E., Ahn, Y., Herrington, A., & McFadden, E. M. (2010). Seasonal variability in the dynamics of marine-terminating outlet glaciers in Greenland. *Journal of Glaciology*, *56*(198), 601–613. https://doi.org/10.3189/002214310793146232

Hubbard, B., Christoffersen, P., Doyle, S. H., Chudley, T. R., Schoonman, C. M., Law, R., & Bougamont, M. (2021). Borehole-Based Characterization of Deep Mixed-Mode Crevasses at a Greenlandic Outlet Glacier. *AGU Advances*, *2*(2), e2020AV000291. https://doi.org/10.1029/2020AV000291

Humbert, A., Helm, V., Zeising, O., Neckel, N., Braun, M. H., Khan, S. A., et al. (2025). Insights into supraglacial lake drainage dynamics: triangular fracture formation, reactivation and long-lasting englacial features. *The Cryosphere*, *19*(8), 3009–3032. https://doi.org/10.5194/tc-19-3009-2025

Jiménez, S., & Duddu, R. (2018). On the evaluation of the stress intensity factor in calving models using linear elastic fracture mechanics. *Journal of Glaciology*, *64*(247), 759–770. https://doi.org/10.1017/jog.2018.64

Kendrick, A. K., Schroeder, D. M., Chu, W., Young, T. J., Christoffersen, P., Todd, J., et al. (2018). Surface Meltwater Impounded by Seasonal Englacial Storage in West Greenland. *Geophysical Research Letters*, *45*(19), 10,474-10,481. https://doi.org/10.1029/2018GL079787

Khan, N., Poinar, K., Briner, J. P., Nowicki, S., Mejia, J., & Verne, M. (2025). Crevasse locations and meltwater delivery to the bed in Pakitsoq, Greenland: Results from MimiNet, a new deep-learning model for crevasse detection. Retrieved from https://eartharxiv.org/repository/view/9580/

Koziol, C., & Arnold, N. (2018). Modelling seasonal meltwater forcing of the velocity of the Greenland Ice Sheet. https://doi.org/10.5194/tc-12-971-2018

Koziol, C., Arnold, N., Pope, A., & Colgan, W. (2017). Quantifying supraglacial meltwater pathways in the Paakitsoq region, West Greenland. *Journal of Glaciology*, 1–13. https://doi.org/10.1017/jog.2017.5

Krawczynski, M. J., Behn, M. D., Das, S. B., & Joughin, I. (2009). Constraints on the lake volume required for hydro-fracture through ice sheets. *Geophysical Research Letters*, *36*(10). https://doi.org/10.1029/2008GL036765

Lai, C.-Y., Kingslake, J., Wearing, M. G., Chen, P.-H. C., Gentine, P., Li, H., et al. (2020). Vulnerability of Antarctica's ice shelves to meltwater-driven fracture. *Nature*, *584*(7822), 574–578. https://doi.org/10.1038/s41586-020-2627-8

Lampkin, D. J., Amador, N., Parizek, B. R., Farness, K., & Jezek, K. (2013). Drainage from water-filled crevasses along the margins of Jakobshavn Isbræ: A potential catalyst for catchment expansion. *Journal of Geophysical Research: Earth Surface*, *118*(2), 795–813. https://doi.org/10.1002/jgrf.20039

Lampkin, D. J., Parizek, B., Larour, E. Y., Seroussi, H., Joseph, C., & Cavanagh, J. P. (2018). Toward Improved Understanding of Changes in Greenland Outlet Glacier Shear Margin Dynamics in a Warming Climate. *Frontiers in Earth Science*, *6*. https://doi.org/10.3389/feart.2018.00156

Law, R. (2025). Rapid Hydrofracture of Icy Moon Shells: Insights From Glaciology. *Journal of Geophysical Research: Planets*, *130*(4), e2024JE008403. https://doi.org/10.1029/2024JE008403

Law, R., Christoffersen, P., Hubbard, B., Doyle, S. H., Chudley, T. R., Schoonman, C. M., et al. (2021). Thermodynamics of a fast-moving Greenlandic outlet glacier revealed by fiber-optic distributed temperature sensing. *Science Advances*, *7*(20), eabe7136. https://doi.org/10.1126/sciadv.abe7136

Li, L., & Pomeroy, J. W. (1997). Probability of occurrence of blowing snow. *Journal of Geophysical Research: Atmospheres*, *102*(D18), 21955–21964. https://doi.org/10.1029/97JD01522

Lutz, K., Bahrami, Z., & Braun, M. (2023). Supraglacial Lake Evolution over Northeast Greenland Using Deep Learning Methods. *Remote Sensing*, *15*(17), 4360. https://doi.org/10.3390/rs15174360

McGrath, D., Colgan, W., Steffen, K., Lauffenburger, P., & Balog, J. (2011). Assessing the summer water budget of a moulin basin in the Sermeq Avannarleq ablation region, Greenland ice sheet. *Journal of Glaciology*, *57*(205), 954–964. https://doi.org/10.3189/002214311798043735

McInnes, L., & Healy, J. (2017). Accelerated Hierarchical Density Based Clustering. In *2017 IEEE International Conference on Data Mining Workshops (ICDMW)* (pp. 33–42). https://doi.org/10.1109/ICDMW.2017.12

McInnes, L., Healy, J., & Astels, S. (2017). hdbscan: Hierarchical density based clustering. *Journal of Open Source Software*, *2*(11), 205. https://doi.org/10.21105/joss.00205

Mejia, J. Z., Poinar, K., Meyer, C. R., Sommers, A. N., & Chu, W. (2025). Mechanisms for upstream migration of firn aquifer drainage: preliminary observations from Helheim Glacier, Greenland. *Journal of Glaciology*, *71*, e5. https://doi.org/10.1017/jog.2024.78

Moon, T., Joughin, I., Smith, B., van den Broeke, M. R., van de Berg, W. J., Noël, B., & Usher, M. (2014). Distinct patterns of seasonal Greenland glacier velocity. *Geophysical Research Letters*, *41*(20), 7209–7216. https://doi.org/10.1002/2014GL061836

Noël, B., van de Berg, W. J., Lhermitte, S., & van den Broeke, M. R. (2019). Rapid ablation zone expansion amplifies north Greenland mass loss. *Science Advances*, *5*(9), eaaw0123. https://doi.org/10.1126/sciadv.aaw0123

Phillips, T., Rajaram, H., & Steffen, K. (2010). Cryo-hydrologic warming: A potential mechanism for rapid thermal response of ice sheets. *Geophysical Research Letters*, *37*(20). Retrieved from http://onlinelibrary.wiley.com/doi/10.1029/2010GL044397/full

Poinar, K. (2020). Water-filled ditches: Surface expressions of dead crevasses that are not connected to the bed. *ESS Open Archive*. https://doi.org/10.1002/essoar.10505037.1

Poinar, K., & Andrews, L. C. (2021). Challenges in predicting Greenland supraglacial lake drainages at the regional scale. *The Cryosphere*, *15*(3), 1455–1483. https://doi.org/10.5194/tc-15-1455-2021

Poinar, K., Joughin, I., Lilien, D., Brucker, L., Kehrl, L., & Nowicki, S. (2017). Drainage of Southeast Greenland Firn Aquifer Water through Crevasses to the Bed. *Frontiers in Earth Science*, *5*. https://doi.org/10.3389/feart.2017.00005

Poinar, K., Dow, C. F., & Andrews, L. C. (2019). Long-Term Support of an Active Subglacial Hydrologic System in Southeast Greenland by Firn Aquifers. *Geophysical Research Letters*, *46*(9), 4772–4781. https://doi.org/10.1029/2019GL082786

Porter, C., Howat, I., Noh, M.-J., Husby, E., Khuvis, S., Danish, E., et al. (2023). ArcticDEM - Mosaics, Version 4.1 [Data set]. Harvard Dataverse. https://doi.org/10.7910/DVN/3VDC4W

Ravanel, L., Lacroix, E., Le Meur, E., Batoux, P., & Malet, E. (2022). Multiparameter monitoring of crevasses on an Alpine glacier to understand formation and evolution of snow bridges. *Cold Regions Science and Technology*, *203*, 103643. https://doi.org/10.1016/j.coldregions.2022.103643

Reynolds, B., Nowicki, S., & Poinar, K. (2024). Comprehensive Assessment of Stress Calculations for Crevasse Depths and Testing with Crevasse Penetration as Damage. *EGUsphere*, 1–37. https://doi.org/10.5194/egusphere-2024-2424

Reynolds, B., Nowicki, S., & Poinar, K. (2025). Comprehensive assessment of stress calculations for crevasse depths and testing with crevasse penetration as damage. *The Cryosphere*, *19*(10), 5045–5073. https://doi.org/10.5194/tc-19-5045-2025

Robin, G. Q. D. (1974). Depth of water-filled crevasses that are closely spaced. *Journal of Glaciology*, *13*(69), 543–543. https://doi.org/10.3189/S0022143000023285

Ronneberger, O., Fischer, P., & Brox, T. (2015). U-Net: Convolutional Networks for Biomedical Image Segmentation. In N. Navab, J. Hornegger, W. M. Wells, & A. F. Frangi (Eds.), *Medical Image Computing and Computer-Assisted Intervention – MICCAI 2015* (pp. 234–241). Cham: Springer International Publishing. https://doi.org/10.1007/978-3-319-24574-4_28

Scholzen, C., Schuler, T. V., & Gilbert, A. (2021). Sensitivity of subglacial drainage to water supply distribution at the Kongsfjord basin, Svalbard. *The Cryosphere*, *15*(6), 2719–2738. https://doi.org/10.5194/tc-15-2719-2021

Schoof, C. (2010). Ice-sheet acceleration driven by melt supply variability. *Nature*, *468*(7325), 803–806. https://doi.org/10.1038/nature09618

Slater, D. A., & Straneo, F. (2022). Submarine melting of glaciers in Greenland amplified by atmospheric warming. *Nature Geoscience*, 1–6. https://doi.org/10.1038/s41561-022-01035-9

Slater, T., Shepherd, A., McMillan, M., Leeson, A., Gilbert, L., Muir, A., et al. (2021). Increased variability in Greenland Ice Sheet runoff from satellite observations. *Nature Communications*, *12*(1), 6069. https://doi.org/10.1038/s41467-021-26229-4

Sommers, A. N., Meyer, C. R., Poinar, K., Mejia, J., Morlighem, M., Rajaram, H., et al. (2024). Velocity of Greenland's Helheim Glacier Controlled Both by Terminus Effects and Subglacial Hydrology With Distinct Realms of Influence. *Geophysical Research Letters*, *51*(15), e2024GL109168. https://doi.org/10.1029/2024GL109168

Stevens, L. A., Behn, M. D., McGuire, J. J., Das, S. B., Joughin, I., Herring, T., et al. (2015). Greenland supraglacial lake drainages triggered by hydrologically induced basal slip. *Nature*, *522*(7554), 73–76. https://doi.org/10.1038/nature14480

Stevens, L. A., Nettles, M., Davis, J. L., Creyts, T. T., Kingslake, J., Ahlstrøm, A. P., & Larsen, T. B. (2022). Helheim Glacier diurnal velocity fluctuations driven by surface melt forcing. *Journal of Glaciology*, *68*(267), 77–89. https://doi.org/10.1017/jog.2021.74

Stevens, L. A., Das, S. B., Behn, M. D., McGuire, J. J., Lai, C.-Y., Joughin, I., et al. (2024). Elastic Stress Coupling Between Supraglacial Lakes. *Journal of Geophysical Research: Earth Surface*, *129*(5), e2023JF007481. https://doi.org/10.1029/2023JF007481

Surawy-Stepney, T., Hogg, A. E., Cornford, S. L., & Hogg, D. C. (2023). Mapping Antarctic crevasses and their evolution with deep learning applied to satellite radar imagery. *The Cryosphere*, *17*(10), 4421–4445. https://doi.org/10.5194/tc-17-4421-2023

Tada, H., Paris, P. C., & Irwin, G. R. (2000). *The Stress Analysis of Cracks Handbook, Third Edition*. ASME Press. https://doi.org/10.1115/1.801535

Vaughan, D. G. (1993). Relating the occurrence of crevasses to surface strain rates. *Journal of Glaciology*, *39*(132), 255–266. https://doi.org/10.3189/S0022143000015926

van der Veen, C. J. (1998). Fracture mechanics approach to penetration of surface crevasses on glaciers. *Cold Regions Science and Technology*, *27*(1), 31–47. https://doi.org/10.1016/S0165-232X(97)00022-0

van der Veen, C. J. (2007). Fracture propagation as means of rapidly transferring surface meltwater to the base of glaciers. *Geophysical Research Letters*, *34*(1). https://doi.org/10.1029/2006GL028385

Vijay, S., Khan, S. A., Kusk, A., Solgaard, A. M., Moon, T., & Bjørk, A. A. (2019). Resolving seasonal ice velocity of 45 Greenlandic glaciers with very high temporal details. *Geophysical Research Letters*, *46*(3), 1485–1495. https://doi.org/10.1029/2018GL081503

Weertman, J. (1973). Can a water-filled crevasse reach the bottom surface of a glacier. *IASH Publ*, *95*, 139–145.

Williamson, A. G., Willis, I. C., Arnold, N. S., & Banwell, A. F. (2018). Controls on rapid supraglacial lake drainage in West Greenland: an Exploratory Data Analysis approach. *Journal of Glaciology*, 1–19. https://doi.org/10.1017/jog.2018.8

Williamson, A. G., Banwell, A. F., Willis, I. C., & Arnold, N. S. (2018). Dual-satellite (Sentinel-2 and Landsat 8) remote sensing of supraglacial lakes in Greenland. *The Cryosphere*, *12*(9), 3045–3065. https://doi.org/10.5194/tc-12-3045-2018

Yang, K., Smith, L. C., Sole, A., Livingstone, S. J., Cheng, X., Chen, Z., & Li, M. (2019). Supraglacial rivers on the northwest Greenland Ice Sheet, Devon Ice Cap, and Barnes Ice Cap mapped using Sentinel-2 imagery. *International Journal of Applied Earth Observation and Geoinformation*, *78*, 1–13. https://doi.org/10.1016/j.jag.2019.01.008

Young, T. J., Christoffersen, P., Bougamont, M., Tulaczyk, S. M., Hubbard, B., Mankoff, K. D., et al. (2022). Rapid basal melting of the Greenland Ice Sheet from surface meltwater drainage. *Proceedings of the National Academy of Sciences*, *119*(10), e2116036119. https://doi.org/10.1073/pnas.2116036119

Zhang, W., Yang, K., Smith, L. C., Wang, Y., van As, D., Noël, B., et al. (2023). Pan-Greenland mapping of supraglacial rivers, lakes, and water-filled crevasses in a cool summer (2018) and a warm summer (2019). *Remote Sensing of Environment*, *297*, 113781. https://doi.org/10.1016/j.rse.2023.113781

Zuhr, A. M., Münch, T., Steen-Larsen, H. C., Hörhold, M., & Laepple, T. (2021). Local-scale deposition of surface snow on the Greenland ice sheet. *The Cryosphere*, *15*(10), 4873–4900. https://doi.org/10.5194/tc-15-4873-2021